Chinese Journal of Aeronautics 24 (2011) 687-700

Contents lists available at ScienceDirect

Chinese Journal of Aeronautics

journal homepage: www.elsevier.com/locate/cja

A Model to Predict Stall Inception of Transonic Axial Flow Fan/Compressors

SUN Xiaofeng*, SUN Dakun, YU Weiwei

School of Jet Propulsion, Beihang University, Beijing 100191, China

Received 13 July 2011; revised 15 August 2011; accepted 27 September 2011

Abstract

A stall inception model for transonic fan/compressors is presented in this paper. It can be shown that under some assumptions the solution of unsteady flow field consists of pressure wave which propagates upstream or downstream, vortex wave and entropy wave convected with the mean flow speed. By further using the mode-matching technique and applying the conservation law and conditions reflecting the loss characteristics of a compressor in the inlet and outlet of the rotor or stator blade rows, a group of homogeneous equations can be obtained from which the stability equation can be derived. Based on the analysis of the unsteady phenomenon caused by casing treatments, the function of casing treatments has been modeled by a wall impedance condition which has been included in the stability model through the eigenvalues and the corresponding eigenfunctions of the system. Besides, the effect of shock waves in cascade channel on the stability prediction is also considered in the stall inception model. Finally, some numerical analysis and experimental investigation are also conducted with emphasis on the mutual comparison.

Keywords: stability model; rotating stall; stall inception; transonic compressor; unsteady flow

1. Introduction

Considerable work was done in the past decades on investigating the phenomenon of rotating stall in axial flow compressors. These studies focused on two major respects. The first respect mainly puts emphasis on the prediction of propagation speed and number of stall cell, the study of non-linear development of stall cell and the numerical simulation, measurement of the structure of stall cell and so on. The second is about the investigations related to the inception condition of rotating stall. Especially the latter has become increasingly important since the concept of active control of rotating stall and surge was put forward [1-4]. The study about the precursor and inception condition of rotating stall has thus become one of the important subjects in recent theoretical and experimental research work of compressor stability. However there are many important problems still to be overcome. Firstly, how to understand the effect of the shock waves in transonic compressors on the generation and development of rotating stall is still a problem unsolved in the existing theoretical models. Secondly, in the design stage of a fan/compressor, its performance like the characteristic line is usually obtained on the basis of steady computational fluid dynamics (CFD) calculation or other empirical methods, and how to apply the stability model to check the stall inception point of the characteristic line in order to relatively accurately determine stall margin is also a problem of common interest for turbomachinery designers. In addition, what role the wall boundary condition plays in the change of stall inception is still lack of convincing conclusions. It is believed that any relevant progress for this aspect may result in a better understanding of some casing treat-

*Corresponding author. Tel.: +86-10-82317408.
E-mail address: sunxf@buaa.edu.cn
Foundation item: National Natural Science Foundation of China (50736007, 51010007)

doi: 10.1016/S1000-9361(11)60081-2

ments. Obviously, to gain insight into these problems, a transonic flow stability model including these factors is needed.

In general, there are two different kinds of work to study the stall inception in compressors. One is to describe the compressor stability as an eigenvalue problem, while the stability can be judged by the imaginary part of the corresponding eigenvalues. The other is to directly solve Euler or Navier-Stokes equations as an initial boundary value problem to obtain the information related to the inception condition [5-9]. The latter's advantage is that this type of work can include the effect of more aerodynamic and geometrical parameters on the physical phenomena involved than the eigenvalue approach. However, there are no common rules to be followed about how to introduce the initial perturbations outside or inside the computational domain to stimulate the stall inception or precursor. Therefore whether or not one can obtain a rapid and reliable result about the stall inception along the way will strongly depend on researcher's experience and an affordable computational cost to a great extent. On the other hand, it is noted that for a dynamic system, its stability will depend on the response to a small perturbation outside the system. Mathematically, what one should do for this kind of analysis is to solve the corresponding eigenvalue equation in order to judge whether the system is stable or not. In fact, we can see that most of earlier work in the studies of the stall inception was to establish various eigenvalue models. Besides, the development of eigenvalue models in a compressible system has experienced a different stage since the 1970s. Nenni and Ludwig [10] extended the channel flow theory presented by Sears [11] so as to include the effects of more aerodynamic and geometrical parameters of compressor rotors. Their work also resulted in an analytical expression for the inception condition of rotating stall. The work was soon extended to two-dimensional compressible flow case but no relevant numerical results were reported in Ref. [12]. Greitzer [13] and Moore [14-15] presented a stability model of compressor system in different approaches. The model can not only be used to predict the inception condition of stall and surge but also to study the non-linear development of stall cells [16]. In recent years, the compressible flow stability model of rotating stall in multi-stage compressors is also investigated based on solving linearized Euler equations [17-18]. Furthermore, to authors' knowledge, there were some attempts to set up three-dimensional stability model of compressors in the previous work. Ludwig and Nenni developed a three-dimensional incompressible flow stability model of rotating stall but not any numerical results were presented in Ref. [12]. Takata and Nagashima [19] studied the rotating stall in three-dimensional blade rows with emphasis on the effects of non-uniform flow or shear flow on the stall inception. Besides, Gordon [20] presented a three-dimensional incompressible stability model in annular domain to study the inception of rotating stall in compressors. These investigations fully show the progress in how to include three-dimensional effect in the stability model of fan/compressors. However, these models are still lack of the connection with the change of wall boundary condition, naturally being incapable of handling how the wall boundary condition affects the inception and evolution of the stall precursor. Besides, the effect of shock waves in a transonic compressor has not yet been found in the existing eigenvalue models.

In the present study, we first simplify the real annular cascade as a liner cascade with tip and hub plates. The shortcomings of this simplification are to neglect the effect of centrifugal forces and radial steady flow in the cascade channel on the stability, while the advantages is to include the effect of three-dimensional perturbations on the stability. It is also noted that such simplification could be found in different applications for turbomachinery [19,21-22]. In particular, the present three-dimensional model is obtained by the following steps. First, the flow can be assumed to be small perturbation since emphasis is placed on the inception condition of rotating stall. So the flow fields can be described by three-dimensional compressible linearized Euler equations. Under the conditions of uniform flow, the equations can be solved in three different regions, i.e. upstream and downstream fields of cascade, cascade field with three-dimensional semi-actuator disk approximation [22-23], and each flow region is solved separately to satisfy the boundary conditions at both tip and hub walls. It can be shown that the solution consists of pressure wave which propagates upstream or downstream, vortex wave and entropy wave convected with the mean flow speed. By further using the mode-matching technique [24-26] and applying the conservation law and conditions reflecting the loss characteristics of a compressor in the inlet and outlet of the rotor or stator blade rows, a group of homogeneous equations will yield from which the stability equations can be obtained. In addition, when there are shock waves in cascade channel, a normal shock wave model [27] is used to be included in the stability model with emphasis on its effect of various wave reflections. It is well known that the solution of eigenvalue equation is extremely difficult even though you have derived the stability equation for stall inception. Nyquist stability criterion may be used to judge whether there is a meaningful eigenvalue but it cannot be used to determine its exact value, such as unsteady frequency. With the development of complex function theory in recent decades, a new method called winding number integral approach was applied to determine the roots of dispersion equations [28-29], which shows great potentials over the existing methods. In this study, we have investigated how to extend the winding number integral approach to be suitable for the present stability equations in matrix form.

On the basis of the present model, we have carried out various stability predictions for both subsonic and transonic fan/compressors. Especially, we have also made the relevant experimental investigation, which shows that a reasonable stability prediction for fan/compressors can be realized using either the experimental data (characteristics and losses, et al.) or calculating data from CFD. In the following text, we will first introduce how to derive the model and then the relevant numerical studies to the model are presented.

2. Theoretical Model of Stall Inception

2.1. Analytical solutions of basic equations in an unbladed region

As shown in Fig. 1, a linear cascade of blades is modeled by the three-dimensional semi-actuator disk composed of flat-plate airfoils with chord length c, spacing s and stagger angle θ. The x, y and z represent axial, circumferential and radial coordinates, respectively. This model assumes that the flow disturbances have wave lengths in its circumferential direction which are large compared with the blade spacing. There is no restriction upon the ratio of blade chord length to wave length. A compressible, inviscid, non-heat-conductive uniform flow is considered. As to casing walls, the hub side (z=0) is assumed rigid while the tip side (z=h, where h is the radial blade height) is assumed to have a finite acoustic impedance.

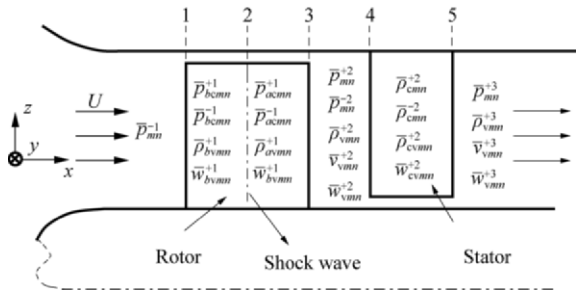

Fig. 1 Schematic of a compressor stage unwrapped in circumferential direction.

The governing equations for a small disturbance problem are the linearized Euler equations as follows, which reflect the conservation relations for mass, momentum, and energy.

$$\frac{\partial \rho}{\partial t}+U\frac{\partial \rho}{\partial x}+V\frac{\partial \rho}{\partial y}+\rho_0\left(\frac{\partial u}{\partial x}+\frac{\partial v}{\partial x}+\frac{\partial w}{\partial z}\right)=0 \quad (1)$$

$$\frac{\partial u}{\partial t}+U\frac{\partial u}{\partial x}+V\frac{\partial u}{\partial y}=-\frac{1}{\rho_0}\frac{\partial p}{\partial x} \quad (2)$$

$$\frac{\partial v}{\partial t}+U\frac{\partial v}{\partial x}+V\frac{\partial v}{\partial y}=-\frac{1}{\rho_0}\frac{\partial p}{\partial y} \quad (3)$$

$$\frac{\partial w}{\partial t}+U\frac{\partial w}{\partial x}+V\frac{\partial w}{\partial y}=-\frac{1}{\rho_0}\frac{\partial p}{\partial z} \quad (4)$$

$$\frac{1}{p_0}\left(\frac{\partial p}{\partial t}+U\frac{\partial p}{\partial x}+V\frac{\partial p}{\partial y}\right)-\frac{k}{\rho_0}\left(\frac{\partial \rho}{\partial x}+U\frac{\partial \rho}{\partial x}+V\frac{\partial \rho}{\partial z}\right)=0 \quad (5)$$

where p, ρ, u, v and w are pressure, density, axial velocity, circumferential velocity and radial velocity, k the specific heat ratio. p_0, ρ_0, U and V represent corresponding mean flow parameters. From Eqs. (1)-(5), it can be shown that fluctuating variables related to pressure will satisfy the wave equation in the form of

$$(1-Ma_x^2)\frac{\partial^2 p}{\partial x^2}-2Ma_xMa_y\frac{\partial^2 p}{\partial x\partial y}+(1-Ma_y^2)\frac{\partial^2 p}{\partial y^2}+\frac{\partial^2 p}{\partial z^2}-\frac{1}{a_0^2}\frac{\partial^2 p}{\partial z^2}-\frac{2Ma_x}{a_0}\frac{\partial^2 p}{\partial x\partial t}-\frac{2Ma_y}{a_0}\frac{\partial^2 p}{\partial y\partial t}=0 \quad (6)$$

where Ma_x and Ma_y are axial and circumferential Mach numbers, a_0 the sound speed.

Assume that solution of Eq. (6) is

$$p(x,y,z,t)=\sum_{m=-\infty}^{+\infty}p_m(x)\psi_m(z)\mathrm{e}^{\mathrm{i}(\beta_m y+\omega t)} \quad (7)$$

where m is the circumferential mode number, or ordinal number of harmonic, β_m the circumferential wave number, $\psi_m(z)$ the radial eigenfunction, ω the eigenfrequency of the system. According to periodic condition it can be shown that β_m can be expressed as

$$\beta_m=\frac{m}{r_\mathrm{m}} \quad (8)$$

where r_m is the mean radius length. Obviously the wall boundary condition shown in Fig. 1 will result in

$$\psi_m(z)=\cos(kz) \quad (9)$$

for a hard wall condition

$$\left.\frac{\partial \psi_m(z)}{\partial z}\right|_{z=0,z=h}=0 \quad (10)$$

So the radial wave number k_n for hard wall can be solved as

$$k_n=\frac{(n-1)\pi}{h} \quad (n=1, 2, \cdots) \quad (11)$$

where n is the radial mode number. A boundary condition [30-31] for "soft" wall was verified to satisfy

$$\frac{\partial p}{\partial z}\pm\mathrm{i}A_z k_0\left(1+Ma_x\frac{\alpha}{k_0}+Ma_y\frac{\beta}{k_0}\right)^2 p\Big|_{z=h}=0 \quad (12)$$

where A_z is the acoustic admittance of the wall and α is the axial wave number, while $k_0=\omega/a_0$.

Besides, it should be pointed out that the modeling of the admittance caused by the casing treatment covered with perforated plates or slots may be carried out on the basis of the existing vortex-sound (pressure wave) models [31-39].

In general the radial wave number which is obtained by solving the above equation will be related to the

circumferential wave number β_m. For an appointed β_m, there will be a group of eigenvalues that can be expressed as k_{mn}(n=1, 2,⋯). So for the most general case, Eq. (7) can be expressed as

$$p(x,y,z,t)=\sum_{m=-\infty}^{+\infty}\sum_{n=1}^{+\infty}p_{mn}(x)\psi_{mn}(z)\mathrm{e}^{\mathrm{i}(\beta_m y+\omega t)} \tag{13}$$

Substituting Eq. (13) into Eq. (6) yields

$$p^j(x,y,z,t)=\sum_{m=-\infty}^{+\infty}\sum_{n=1}^{+\infty}\left(\overline{p}_{mn}^{+j}\psi_{mn}^{+j}(z)\mathrm{e}^{\mathrm{i}\alpha_{mn}^{+j}(x-x^j)}+\overline{p}_{mn}^{-j}\psi_{mn}^{-j}(z)\mathrm{e}^{\mathrm{i}\alpha_{mn}^{-j}(x-x^j)}\right)\mathrm{e}^{\mathrm{i}(\beta_m y+\omega t)} \tag{14}$$

where two axial wave numbers are

$$\alpha_{mn}^{-j}=\frac{Ma_x k_y+\sqrt{k_y^2-(1-Ma_x^2)(\beta_m^2+(k_{mn}^{-j})^2)}}{1-Ma_x^2} \tag{15}$$

$$\alpha_{mn}^{+j}=\frac{Ma_x k_y-\sqrt{k_y^2-(1-Ma_x^2)(\beta_m^2+(k_{mn}^{+j})^2)}}{1-Ma_x^2} \tag{16}$$

$$k_y=Ma_y\beta_m+\frac{\omega}{a_0} \tag{17}$$

where $\overline{p}_{mn}$ is the wave amplitude and x^j is axial coordinate for an arbitrary reference plane, and "+j" and "–j" represent the waves traveling downstream and upstream from the plane x^j, respectively.

2.1.1. Vortex wave

Since the vortex wave will not cause the pressure variation, the solutions related to vortex mode can be given by the homogeneous form of Eqs. (2)-(3). It has been noted that fluctuating radial velocity w is composed of two parts: one is the contribution by the pressure wave w_p and the other is by the vortex wave w_v. Since the wave lengthes of the pressure wave and the vortex wave are different from each other, w_v can be shown not to contribute to the left hand side of Eq. (12). For this reason [22], w_v is concluded to satisfy the following condition on the non-rigid wall

$$w_\mathrm{v}\,|_{z=0,z=h}=0 \tag{18}$$

The corresponding solutions for the homogeneous form of Eqs. (2)-(3) are

$$u_\mathrm{v}^j(x,y,z,t)=\sum_{m=-\infty}^{+\infty}\sum_{n=1}^{+\infty}\overline{u}_{\mathrm{v}mn}^{+j}\psi_{\mathrm{v}mn}^{+j}(z)\mathrm{e}^{-\mathrm{i}\frac{\omega+V^j\beta_m}{U^j}(x-x^j)}\mathrm{e}^{\mathrm{i}(\beta_m y+\omega t)} \tag{19}$$

$$v_\mathrm{v}^j(x,y,z,t)=\sum_{m=-\infty}^{+\infty}\sum_{n=1}^{+\infty}\overline{v}_{\mathrm{v}mn}^{+j}\psi_{\mathrm{v}mn}^{+j}(z)\mathrm{e}^{-\mathrm{i}\frac{\omega+V^j\beta_m}{U^j}(x-x^j)}\mathrm{e}^{\mathrm{i}(\beta_m y+\omega t)} \tag{20}$$

$$w_\mathrm{v}^j(x,y,z,t)=\sum_{m=-\infty}^{+\infty}\sum_{n=1}^{+\infty}\overline{w}_{\mathrm{v}mn}^{+j}\phi_{\mathrm{v}mn}^{+j}(z)\mathrm{e}^{-\mathrm{i}\frac{\omega+V^j\beta_m}{U^j}(x-x^j)}\mathrm{e}^{\mathrm{i}(\beta_m y+\omega t)} \tag{21}$$

where $\overline{u}_{\mathrm{v}mn}^{+j}$, $\overline{v}_{\mathrm{v}mn}^{+j}$ and $\overline{w}_{\mathrm{v}mn}^{+j}$ are the wave amplitudes, the eigenfunctions are

$$\psi_{\mathrm{v}mn}^{+j}(z)=\cos(k_{\mathrm{v}mn}^{+j}z) \tag{22}$$

$$\phi_{\mathrm{v}mn}^{+j}(z)=\sin(k_{\mathrm{v}mn}^{+j}z) \tag{23}$$

2.1.2. Entropy wave

Since the entropy and the vorticity are related by Crocco's theorem, there must be the solution of the entropy wave with the solution of the vorticity wave inside the gap and blade row. It can be shown that the entropy wave relates to a density fluctuation, or, to temperature fluctuation since no pressure fluctuation is accompanied by this wave. So according to energy equation, the density related to entropy variation will be determined by the equation:

$$\frac{\partial\rho}{\partial t}+U\frac{\partial\rho}{\partial x}+V\frac{\partial\rho}{\partial y}=0 \tag{24}$$

Further the walls are assumed to be adiabatic to such fluctuation, so the adiabatic condition of boundary walls is described as

$$\left.\frac{\partial T}{\partial z}\right|_{z=0,z=h}=0 \tag{25}$$

where T is the temperature.

The solution of Eq. (24) is

$$\rho_\mathrm{v}^j(x,y,z,t)=\sum_{m=-\infty}^{+\infty}\sum_{n=1}^{+\infty}\overline{\rho}_{\mathrm{v}mn}^{+j}\psi_{\mathrm{v}mn}^{+j}(z)\mathrm{e}^{-\mathrm{i}\frac{\omega+V^j\beta_m}{U^j}(x-x^j)}\mathrm{e}^{\mathrm{i}(\beta_m y+\omega t)} \tag{26}$$

where $\overline{\rho}_{\mathrm{v}mn}$ is the wave amplitude. With the above basic solutions, it is shown below.

The fluctuating density is

$$\rho^j(x,y,z,t)=\sum_{m=-\infty}^{+\infty}\sum_{n=1}^{+\infty}\left[-\frac{1}{\alpha_0^2}\left(\overline{p}_{mn}^{+j}\psi_{mn}^{+j}(z)\mathrm{e}^{\mathrm{i}\alpha_{mn}^{+j}(x-x^j)}+\overline{p}_{mn}^{-j}\psi_{mn}^{-j}(z)\mathrm{e}^{\mathrm{i}\alpha_{mn}^{-j}(x-x^j)}\right)+\overline{\rho}_{\mathrm{v}mn}^{+j}\psi_{\mathrm{v}mn}^{+j}(z)\mathrm{e}^{-\mathrm{i}\frac{\omega+V^j\beta_m}{U^j}(x-x^j)}\right]\mathrm{e}^{\mathrm{i}(\beta_m y+\omega t)} \tag{27}$$

The fluctuating axial velocity is

$$u^j(x,y,z,t)=\sum_{m=-\infty}^{+\infty}\sum_{n=1}^{+\infty}\left[-\frac{1}{\rho_0^j}\left(\frac{\overline{p}_{mn}^{+j}\alpha_{mn}^{+j}\mathrm{e}^{\mathrm{i}\alpha_{mn}^{+j}(x-x^j)}}{\omega+\alpha_{mn}^{+j}U^j+\beta_m V^j}\psi_{mn}^{+j}(z)+\frac{\overline{p}_{mn}^{-j}\alpha_{mn}^{-j}\mathrm{e}^{\mathrm{i}\alpha_{mn}^{-j}(x-x^j)}}{\omega+\alpha_{mn}^{-j}U^j+\beta_m V^j}\psi_{mn}^{-j}(z)\right)+\left(\frac{\overline{v}_{\mathrm{v}mn}^{+j}\beta_m U^j}{\omega+\beta_m V^j}-\frac{\mathrm{i}\overline{w}_{\mathrm{v}mn}^{+j}k_{mn}^{+j}U^j}{\omega+\beta_m V^j}\right)\psi_{\mathrm{v}mn}^{+j}(z)\mathrm{e}^{-\mathrm{i}\frac{\omega+V^j\beta_m}{U^j}(x-x^j)}\right]\cdot$$

$$\mathrm{e}^{\mathrm{i}(\beta_m y+\omega t)} \tag{28}$$

The fluctuating circumferential velocity is

$$v^j(x,y,z,t)=\sum_{m=-\infty}^{+\infty}\sum_{n=1}^{+\infty}\left[-\frac{1}{\rho_0^j}\left(\frac{\overline{p}_{mn}^{+j}\beta_{mn}^{+j}\mathrm{e}^{\mathrm{i}\alpha_{mn}^{+j}(x-x^j)}}{\omega+\alpha_{mn}^{+j}U^j+\beta_m V^j}\psi_{mn}^{+j}(z)+\frac{\overline{p}_{mn}^{-j}\beta_{mn}^{-j}\mathrm{e}^{\mathrm{i}\alpha_{mn}^{-j}(x-x^j)}}{\omega+\alpha_{mn}^{-j}U^j+\beta_m V^j}\psi_{mn}^{-j}(z)\right)+\overline{v}_{\mathrm{v}mn}^{+j}\psi_{\mathrm{v}mn}^{+j}(z)\mathrm{e}^{-\mathrm{i}\frac{\omega+V^j\beta_m}{U^j}(x-x^j)}\right]\mathrm{e}^{\mathrm{i}(\beta_m y+\omega t)} \tag{29}$$

The fluctuating radial velocity is

$$w^j(x,y,z,t)=\sum_{m=-\infty}^{+\infty}\sum_{n=1}^{+\infty}\left[-\frac{1}{\rho_0^j}\left(\frac{\overline{p}_{mn}^{+j}k_{mn}^{+j}\mathrm{e}^{\mathrm{i}\alpha_{mn}^{+j}(x-x^j)}}{\omega+\alpha_{mn}^{+j}U^j+\beta_m V^j}\phi_{mn}^{+j}(z)+\frac{\overline{p}_{mn}^{-j}k_{mn}^{-j}\mathrm{e}^{\mathrm{i}\alpha_{mn}^{-j}(x-x^j)}}{\omega+\alpha_{mn}^{-j}U^j+\beta_m V^j}\phi_{mn}^{-j}(z)\right)+\overline{w}_{\mathrm{v}mn}^{+j}\phi_{\mathrm{v}mn}^{+j}(z)\mathrm{e}^{-\mathrm{i}\frac{\omega+V^j\beta_m}{U^j}(x-x^j)}\right]\mathrm{e}^{\mathrm{i}(\beta_m y+\omega t)} \tag{30}$$

The eigenfunctions of radial velocity are different from the others because the radial component of velocity must be zero at the hard wall. It is obtained from Eq. (4)

$$\phi_{mn}^{\pm j}(z)=\phi_{\mathrm{v}mn}^{\pm j}(z)=\sin(k_{mn}^{\pm j}z) \tag{31}$$

There is no difference between k_{mn}^{+j} and k_{mn}^{-j} under the condition of hard wall.

2.2. Analytical solutions of basic equations in a bladed region

First, it is assumed that cascade can be simplified as three-dimensional semi-actuator disk. This means that in the cascade the main flow is considered to be one-dimensional, or to be channel flow, which has radial fluctuating velocity component and chordwise fluctuating velocity component but no circumferential fluctuating velocity component in the channel of blades.

Besides it should be noted that the phase change of the wave motion in the cascade direction must coincide with that in the upstream or downstream flow. There the perturbation waves in the channel can be expressed in the form $\mathrm{e}^{\mathrm{i}(\omega t+\alpha_{cmn}x+\beta_m y')}$ with the phase factor $\mathrm{e}^{\mathrm{i}\beta_m y'}$. Further, if moving blade fixed coordinates are used, i.e. $y=y'-\Omega r_{\mathrm{m}}t$ (y' is the rotating coordinate, and Ω the rotating frequency), then the waves in the channel can be expressed in the form of $\mathrm{e}^{\mathrm{i}[(\omega-m\Omega)t+\alpha_{cmn}x+\beta_m y']}$. Under these conditions the solution for bladed region can be obtained. But it is noted that these solutions have similar character like those solutions in unbladed regions. For each harmonic wave or single modes of all perturbation quantities, there are also four coefficients $\overline{p}_{\mathrm{c}mn}^{+k}$, $\overline{p}_{\mathrm{c}mn}^{-k}$, $\overline{w}_{\mathrm{cv}mn}$ and $\overline{\rho}_{\mathrm{cv}mn}^{+k}$, which represent acoustic modes, vortical mode and entropy mode, respectively. There is only one coefficient for vortical mode due to one-dimensionality of the mean flow in the blade passage. Under these conditions, the fluctuating equations are shown below.

The fluctuating pressure is

$$p_{\mathrm{c}}^k(x,y',z,t)=\sum_{m=-\infty}^{+\infty}\sum_{n=1}^{+\infty}\left(\overline{p}_{\mathrm{c}mn}^{+k}\psi_{\mathrm{c}mn}^{+k}(z)\mathrm{e}^{\mathrm{i}\alpha_{\mathrm{c}mn}^{+k}(x-x^k)}+\overline{p}_{\mathrm{c}mn}^{-k}\psi_{\mathrm{c}mn}^{-k}(z)\mathrm{e}^{\mathrm{i}\alpha_{\mathrm{c}mn}^{-k}(x-x^k)}\right)+\mathrm{e}^{\mathrm{i}(\omega-m\Omega)t+\beta_m y'} \tag{32}$$

The fluctuating density is

$$\rho_{\mathrm{c}}^k(x,y',z,t)=\sum_{m=-\infty}^{+\infty}\sum_{n=1}^{+\infty}\left[\frac{1}{(a_0^k)^2}\left(\overline{p}_{\mathrm{c}mn}^{+k}\psi_{\mathrm{c}mn}^{+k}(z)\mathrm{e}^{\mathrm{i}\alpha_{\mathrm{c}mn}^{+k}(x-x^k)}+\overline{p}_{\mathrm{c}mn}^{-k}\psi_{\mathrm{c}mn}^{-k}(z)\mathrm{e}^{\mathrm{i}\alpha_{\mathrm{c}mn}^{-k}(x-x^k)}\right)+\overline{\rho}_{\mathrm{cv}mn}^{+k}\psi_{\mathrm{cv}mn}^{+k}(z)\mathrm{e}^{-\mathrm{i}\frac{W_{\mathrm{c}}^k\beta_m\sin\theta^k+\omega-m\Omega}{W_{\mathrm{c}}^k\cos\theta^k}x}\right]\mathrm{e}^{\mathrm{i}(\omega-m\Omega)t+\beta_m y'} \tag{33}$$

The fluctuating chordwise velocity is

$$q_{\mathrm{c}}^k(x,y',z,t)=\sum_{m=-\infty}^{+\infty}\sum_{n=1}^{+\infty}\left[\frac{1}{\rho_0^k}\left(\frac{\overline{p}_{\mathrm{c}mn}^{+k}\alpha_{\mathrm{c}mn}^{+k}\mathrm{e}^{\mathrm{i}\alpha_{\mathrm{c}mn}^{+k}(x-x^k)}}{\omega-m\Omega+\alpha_{\mathrm{c}mn}^{+k}W_{\mathrm{c}}^k}\psi_{\mathrm{c}mn}^{+k}(z)+\frac{\overline{p}_{\mathrm{c}mn}^{-k}\alpha_{\mathrm{c}mn}^{-k}\mathrm{e}^{\mathrm{i}\alpha_{\mathrm{c}mn}^{-k}(x-x^k)}}{\omega-m\Omega+\alpha_{\mathrm{c}mn}^{-k}W_{\mathrm{c}}^k}\psi_{\mathrm{c}mn}^{-k}(z)\right)-\frac{\mathrm{i}\overline{w}_{\mathrm{cv}mn}^{+k}k_{\mathrm{cv}mn}^{+k}W_{\mathrm{c}}^k}{\omega-m\Omega}\cdot\psi_{\mathrm{cv}mn}^{+k}(z)\mathrm{e}^{-\mathrm{i}\frac{W_{\mathrm{c}}^k\beta_m\sin\theta^k+\omega-m\Omega}{W_{\mathrm{c}}^k\cos\theta^k}(x-x^k)}\right]\mathrm{e}^{\mathrm{i}(\omega-m\Omega)t+\beta_m y'} \tag{34}$$

where W is the relative inflow velocity.

The fluctuating radial velocity is

$$w_{\mathrm{c}}^k(x,y',z,t)=\sum_{m=-\infty}^{+\infty}\sum_{n=1}^{+\infty}\left[\frac{1}{\rho_0^k}\left(\frac{\overline{p}_{\mathrm{c}mn}^{+k}k_{\mathrm{c}mn}^{+k}\mathrm{e}^{\mathrm{i}\alpha_{\mathrm{c}mn}^{+k}(x-x^k)}}{\omega-m\Omega+\alpha_{\mathrm{c}mn}^{+k}W_{\mathrm{c}}^k}\phi_{\mathrm{c}mn}^{+k}(z)+\frac{\overline{p}_{\mathrm{c}mn}^{-k}k_{\mathrm{c}mn}^{-k}\mathrm{e}^{\mathrm{i}\alpha_{\mathrm{c}mn}^{-k}(x-x^k)}}{\omega-m\Omega+\alpha_{\mathrm{c}mn}^{-k}W_{\mathrm{c}}^k}\phi_{\mathrm{c}mn}^{-k}(z)\right)-$$

$$\overline{w}_{\mathrm{cv}mn}^{+k}\phi_{\mathrm{cv}mn}^{+k}(z)\mathrm{e}^{-\mathrm{i}\frac{W_{\mathrm{c}}^{k}\beta_m\sin\theta^k+\omega-m\Omega}{W_{\mathrm{c}}^{k}\cos\theta^k}(x-x^k)}\Bigg]\mathrm{e}^{\mathrm{i}(\omega-m\Omega)t+\beta_m y'} \tag{35}$$

It is verified that

$$\alpha_{\mathrm{c}mn}^{\pm k}=\frac{1}{\cos\theta^k}\Bigg[-\beta_m\sin\theta^k+\Big(Ma_{\mathrm{c}}(\omega-m\Omega)\Big/a_0^k\mp\sqrt{(\omega-m\Omega)^2\Big/(a_0^k)^2-(1-Ma_{\mathrm{c}}^2)(k_{\mathrm{c}mn}^{\pm k})^2}\Big)\Big/(1-Ma_{\mathrm{c}}^2)\Bigg] \tag{36}$$

$$\overline{q}_{\mathrm{cv}mn}^{+k}=-\frac{\mathrm{i}k_{\mathrm{cv}mn}^{+k}W_{\mathrm{c}}^{k}}{\omega-m\Omega}\overline{w}_{\mathrm{cv}mn}^{+k} \tag{37}$$

where Ma_{c} is the bladed region Mach number. The radial eigenfunctions are

$$\begin{cases}\psi_{\mathrm{c}mn}^{\pm k}(z)=\cos(k_{\mathrm{c}mn}^{\pm k}z)\\ \psi_{\mathrm{cv}mn}^{+k}(z)=\cos(k_{\mathrm{cv}mn}^{+k}z)\end{cases} \tag{38}$$

$$\begin{cases}\phi_{\mathrm{c}mn}^{\pm k}(z)=\sin(k_{\mathrm{c}mn}^{\pm k}z)\\ \phi_{\mathrm{cv}mn}^{+k}(z)=\sin(k_{\mathrm{cv}mn}^{+k}z)\end{cases} \tag{39}$$

2.3. Stability equation for subsonic flow

The coefficients of perturbation wave in the bladed and unbladed regions need to be coupled via the boundary conditions at the leading edge and trailing edge of the blade.

The boundary conditions of blade row inlet are to be applied to the blade reference frame.

(1) Mass conservation

$$\rho^j U^j+\rho_0^j u^j=(\rho^k W_{\mathrm{c}}{}^k+\rho_0^k q^k)\cos\theta^k \tag{40}$$

(2) Relative total temperature conservation

$$\hat{T}'^j=\hat{T}'^k \tag{41}$$

where $\hat{T}'$ is the relative total temperature. By using state equation $p=\rho RT$, it is easy to change $\hat{T}'^j$ and $\hat{T}'^k$ into the variables related to fluctuating pressure and density.

(3) Continuity of radial velocity

$$w^j=w^k \tag{42}$$

(4) Relative total pressure loss characteristics

The total pressure loss is assumed to occur at the leading edge of the blade. This relation is matched through the relative total pressure loss coefficient ξ which is assumed given by $\xi^k=\xi_{\mathrm{qs}}^k\tan\beta_1^j$ in a quasi-steady manner as a function of the inlet relative flow angle β_1.

$$\xi^k=\frac{p_{\mathrm{t}}^j-p_{\mathrm{t}}^k}{(W^j)^2/2} \tag{43}$$

$$(\xi^k)'=\frac{\partial\xi_{\mathrm{qs}}^k}{\partial\tan\beta_1{}^j} \tag{44}$$

where p_{t} is the relative total pressure loss. The first-order lag equation is used herein to find the dynamic loss response in the form of

$$\tau_{\mathrm{loss}}\frac{\partial\xi^k}{\partial t}=\xi_{\mathrm{qs}}^k-\xi^k \tag{45}$$

where τ_{loss} is the time lag. The time lag used in this work is set to be the time for the convected flow passing through the blade row. Then it is shown that the total pressure loss relation is

$$p_{\mathrm{t}}'^k-p_{\mathrm{t}}'^{j+1}=\frac{1}{1+\mathrm{i}\omega\tau_{\mathrm{loss}}}\Bigg[\xi^k\frac{(W^j)^2}{2}\rho^j+\xi^k\rho_0^j(U^ju^j+V^jv^j)+\xi^{k\prime}\rho_0^j\frac{(W^j)^2}{2U^j}\cdot(v^j-\tan(\beta_1{}^ju^j))\Bigg] \tag{46}$$

On the trailing edge plane, the conservation of mass flow and total enthalpy flow are imposed. In principle, the outlet flow angle from the blade row is generally given as a function of the inlet flow angle and the spanwise position. For simplicity it is assumed here that outlet flow angle β_2 is independent of inlet flow angle β_1, and its value is set to be the cascade stagger angle θ. Then the three components of the velocity, static pressure and density are continuous, so we have five equations at the outlet of blade row.

The leading edge and trailing edge boundary conditions arise nine equations for each blade row and two connected unbladed regions. However, these boundary conditions are not sufficient to determine all the coefficients or the frequency of the precursor wave, which means that boundary conditions at the inlet and outlet of a compressor are needed. This section will illustrate how to close the obtained equations by taking a single blade row as an example.

First, there is no coupling between each circumferential harmonic wave. We will therefore restrict our consideration to a particular circumferential mode number "m". Assuming limited radial mode number "N" is in consideration, then there are $5N$ unknown coefficients in description of the upstream and downstream flow fields in the blade row and $4N$ unknowns in the description of the flow region of the blade row itself. Furthermore, it is noticed that the eigenfunctions are $\cos(k_{mn}z)$ and $\sin(k_{mn}z)$, so if each equation is multiplied by $\cos(k_{mv}z)(v=1, 2, \cdots)$ or $\sin(k_{mv}z)(v=1, 2, \cdots)$, the nine equations could be decoupled to $9N$ equations by using the orthogonality of trigonometric functions. In these equations, each nine equations, which contain just one radial mode, are linearly independent from each other.

Assume that there are no inlet disturbances caused by entropy or vortex and no reflection, then inlet condition yields

$$\begin{cases}\overline{p}_{mn}^{-j}=0, \quad \overline{\rho}_{\mathrm{v}mn}^{+j}=0\\ \overline{v}_{\mathrm{v}mn}^{+j}=0, \quad \overline{w}_{\mathrm{v}mn}^{+j}=0\end{cases} \tag{47}$$

For the outlet of the blade row, assuming that there is no reflection, so

$$\overline{p}_{mn}^{+(j+1)} = 0 \tag{48}$$

By using the five conditions, it is shown that the eigenvalue equation can be derived as

$$\begin{bmatrix} \boldsymbol{G}_{m1} & & & \\ & \boldsymbol{G}_{m1} & & \\ & & \ddots & \\ & & & \boldsymbol{G}_{mN} \end{bmatrix} \begin{bmatrix} \boldsymbol{D}_{m1} \\ \boldsymbol{D}_{m2} \\ \vdots \\ \boldsymbol{D}_{mN} \end{bmatrix} = 0 \tag{49}$$

where $\boldsymbol{G}_{mn}$ and $\boldsymbol{D}_{mn}$ are

$$\begin{cases} \boldsymbol{G}_{mn} = \begin{bmatrix} C_{1,1} & C_{1,2} & \cdots & C_{1,5} & & & \\ \vdots & \vdots & & \vdots & & & \\ C_{4,1} & C_{4,2} & \cdots & C_{4,5} & & & \\ & C_{5,2} & \cdots & C_{5,5} & C_{5,6} & \cdots & C_{5,9} \\ & \vdots & & \vdots & \vdots & & \vdots \\ & C_{9,2} & \cdots & C_{9,5} & C_{9,6} & \cdots & C_{9,9} \end{bmatrix}_{mn} \\ \boldsymbol{D}_{mn} = \begin{bmatrix} \overline{p}_{mn}^{-1} & \overline{p}_{\mathrm{c}mn}^{+1} & \cdots & \overline{v}_{\mathrm{v}mn}^{+2} & \overline{w}_{\mathrm{v}mn}^{+2} \end{bmatrix}^{\mathrm{T}} \end{cases}$$

Eq. (49) is a closed equation. Since it is a homogeneous equation, a non-trivial solution exists if

$$\det(\boldsymbol{G}_{mn}(\omega)) = 0 \tag{51}$$

The obtained ω by solving this equation is a complex variable, the imaginary part of which represents whether the system is stable with positive value or unstable with negative value, and the real part of which determines the perturbation frequency of the precursor wave.

2.4. Stability equation for transonic flow

Semi-actuator disk model usually assumes that there is one mean uniform flow within the channel of blade passage. This assumption is basically acceptable in most cases related to incompressible or high subsonic compressible flow. However, for transonic fan/compressors, our investigation shows that the compressible stability model would fail to predict the onset point of rotating stall if the role of shock waves in cascade is only included in the model in the form of shock loss instead of considering the effect of shock reflection on various pressure waves. Besides, it was founded that if the strong in-passage shock was included with a modified semi-actuator disk approach for an aeroelastic problem [27], the model could predict the inception of supersonic choke flutter and supersonic bending flutter successfully. Although this work described a different unsteady phenomenon in turbomachinery, after all it told us the importance of including the effect of shock waves in cascade passage on pressure wave reflections. Therefore, it is necessary to consider the effect of both shock loss and reflection on various pressure waves in the stability model for transonic fan/compressors. In the following section, we will deal with how to derive the stability equation under this circumstance.

2.4.1. Matching conditions

For the determination of matching conditions in both leading and trailing edges of cascade, some further simplifications and assumptions have to be taken. The first thing is that a normal shock wave is assumed to be at the leading edge perpendicular to the channel-wise direction as shown in Fig. 2. The position of the shock will not be changed with the flow variation in our assumption, but its strength depends on the Mach number in front of the shock wave. This Mach number could be obtained by using the Prandtl-Meyer function with the inlet flow Mach number as input parameter. The inlet relative supersonic flow turns to channel-wise direction through an isentropic process, and this transformation just focuses on the leading edge without total pressure loss. This assumption is somewhat like the definition of "unique incidence", but the differences are that the mass flow is not choked especially when the compressor is approaching to the stall line; in addition the shock wave will not extend outside the leading edge of rotor. Another assumption is that the blade profile loss including the loss generated by the interaction of shock and vortex flow happens at the trailing edge, so does the deviation. So, the matching conditions can be rewritten at leading edge and trailing edge in the following way.

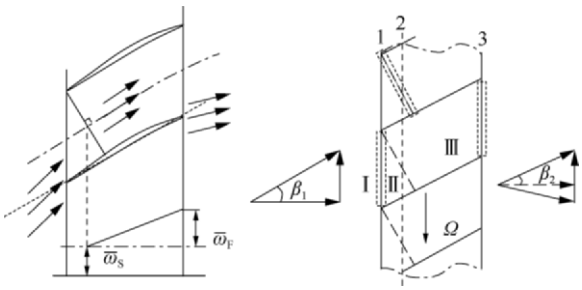

Fig. 2 Schematic of a transonic blade row.

In terms of mass, relative total temperature and relative total pressure conservation relations, and the continuity of radial velocity, we have four equations to be used in the inlet of blade row.

In the outlet, we also have the relative total pressure relation in the form of

$$p_{\mathrm{t}}'^{k} - p_{\mathrm{t}}'^{j+1} = \frac{1}{1+\mathrm{i}\omega\tau_{\mathrm{loss}}}\left[\xi\frac{(W^j)^2}{2}\rho^j + \xi\rho_0^j(U^j u^j + V^j v^j) + \xi'\rho_0^j\frac{(W^j)^2}{2U^j}(v^j - \tan(\beta_1^j u^j))\right] \tag{52}$$

and the deviation condition of outlet flow angle can be written as

$$\tan\beta_2^{j+1} = G(\tan\beta_1^j) \tag{53}$$

$$\frac{v^{j+1}}{U^{j+1}} - \tan\left(\beta_2^{j+1}\frac{u^{j+1}}{U^{j+1}}\right) = \frac{1}{1+\mathrm{i}\omega\tau_{\mathrm{dev}}}\cdot\frac{\partial G}{\partial\tan\beta_1^j}\left(\frac{v^j}{U^j} - \tan\left(\beta_1^j\frac{u^j}{U^j}\right)\right) \quad (54)$$

Besides, according to the continuity of radial velocity, mass, relative temperature conservation relations, we have totally five equations in the outlet of blade row.

It has been seen that the model used different suffix to represent the two parts of the passage, "a" corresponding to subsonic region after the shock, "b", supersonic region before the shock. In fact, the solutions of the unsteady perturbations in each region are obtained in the same way as introduced in the last section. By using the conservation law, the following conditions are used to match the two sets of solutions: matching conditions for in-passage shock.

(1) Mass conservation

$$\rho_{\mathrm{b}}^k W_{\mathrm{b}}^k + \rho_{0\mathrm{b}}^k q_{\mathrm{b}}^k = \rho_{\mathrm{a}}^k W_{\mathrm{a}}^k + \rho_{0\mathrm{a}}^k q_{\mathrm{a}}^k \quad (55)$$

(2) Momentum conservation

$$p_{\mathrm{b}} - p_{\mathrm{a}} = \rho_{\mathrm{a}} W_{\mathrm{a}}^2 - \rho_{\mathrm{b}} W_{\mathrm{b}}^2 \quad (56)$$

(3) Relative total temperature conservation

$$\hat{T}_{\mathrm{b}}'^k = \hat{T}_{\mathrm{a}}'^k \quad (57)$$

(4) Continuity of radial velocity

$$w_{\mathrm{b}}^k = w_{\mathrm{a}}^k \quad (58)$$

2.4.2. Stability equation

Since the number of newly added equations and unknowns is equal, the new eigenvalue equations are still close except that the dimensions are increased. The form of eigenvalue equations is the same as Eq. (51). But the equations' elements, $\boldsymbol{G}_{mn}$, and the unknowns, $\boldsymbol{D}_{mn}$, are different, which are expressed as

$$\begin{cases} \boldsymbol{G}_{mn} = \begin{bmatrix} C_{1,1} & C_{1,2} & \cdots & C_{1,5} & & & & & & \\ \vdots & \vdots & & \vdots & & & & & & \\ C_{4,1} & C_{4,2} & \cdots & C_{4,5} & & & & & & \\ & C_{5,2} & \cdots & C_{5,5} & C_{5,6} & \cdots & C_{5,9} & & & \\ & \vdots & & \vdots & \vdots & & \vdots & & & \\ & C_{8,2} & \cdots & C_{8,5} & C_{8,6} & \cdots & C_{8,9} & & & \\ & & & & C_{9,6} & \cdots & C_{9,9} & C_{9,10} & \cdots & C_{9,13} \\ & & & & \vdots & & \vdots & \vdots & & \vdots \\ & & & & C_{13,6} & \cdots & C_{13,9} & C_{13,10} & \cdots & C_{13,13} \end{bmatrix}_{mn} \\ \boldsymbol{D}_{mn} = \begin{bmatrix} \overline{p}_{mn}^{-1} & \overline{p}_{\mathrm{bc}mn}^{+1} & \cdots & \overline{p}_{\mathrm{ac}mn}^{+1} & \cdots & \overline{v}_{\mathrm{v}mn}^{+2} & \overline{w}_{\mathrm{v}mn}^{+2} \end{bmatrix}^{\mathrm{T}} \end{cases} \quad (59)$$

As to fan/compressors with multi-blade rows or multi-stages, it is convenient to establish the relevant stability equation by using stacking method.

3. Numerical Method for Solving Stability Equation

3.1. Winding number integral approach

It is known that the solution of eigenvalue equation like Eq. (51) has been a difficult problem in various stability models. Newton-Raphson iteration method is widely used to solve such equations, but there is no general rule available to determine its physical solution. In the present investigation, we have tried to use a new kind of approach, i.e., winding number integral approach, to solve the stability equation like Eq. (51), which was never done before for such stability problem. The essence of this approach is a smart application of argument principle and Nyquist stability criterion [28-29]. In fact, Brazier-Smith and Scott [28] firstly demonstrated the efficiency of this approach for determination of the roots of dispersion equations. Ivansson and Karasalo [29] added more features to this method to promote the reliability and efficiency and applied it to research seismo-acoustic wave propagation. It was demonstrated that this method has advantages over other methods that have been proposed, Newton-Raphson iteration methods in particular. However, this approach has been focusing on the solution of dispersion equations with analytical expression, and has not been applied to solving the stability equation like Eq. (51). Therefore, we will first make a brief introduction to the basic principle and then will present an example to demonstrate its success in duct aeroacoustic problem. On the basis of our findings, the present paper will extend this approach to solve the matrix equations for the prediction of rotating stall.

Assert that C is a simple, closed counterclockwise contour, and $f(z)$ is a function which is analytic inside and on C, except possibly for a finite number of poles interior to C, and $f(z)$ has at most a finite number of zeros inside C and none on C, then the definition of winding number integral is

$$S_n = \frac{1}{2\pi\mathrm{i}}\oint_C z^n\frac{f'(z)}{f(z)}\mathrm{d}z \quad (60)$$

If n=0, according to argument principle, then

$$S_0 = \frac{1}{2\pi \mathrm{i}} \oint_C \frac{f'(z)}{f(z)} \mathrm{d}z = N_{\text{zero}}(f) - N_{\text{pole}}(f) = \frac{1}{2\pi} \Delta_C \arg f(z) \tag{61}$$

where N_{zero} is the number of zeros and N_{pole} is the number of poles of $f(z)$ inside C (including multiplicity).

Let us consider a simpler case for n=1. Assume that the number of poles is zero and number of zeros is one, which is z_0, then the winding number integral is

$$S_1 = z_0 = \frac{1}{2\pi \mathrm{i}} \oint_C z \frac{f'(z)}{f(z)} \mathrm{d}z \tag{62}$$

With the two integrals S_0 and S_1, most dispersion equations and eigenvalue equations could be solved with splitting of the search region into subregions such that each subregion contains no more than one root.

On the basis of the above statement, consider a fixed rectangular region R in the complex z plane where roots of an analytic function $f(z)$ are to be found. The first step was to compute S_0 of the analytic function around the boundary of the region R. According to the value of S_0, an adaptive rectangle halving based on zero counts within subrectangles is used. The rectangle halving strategy produces a stack of non-overlapping rectangles $R_1, R_2, \cdots, R_n$, where $R_j \subset R, j=1, 2, \cdots, n$. The union of the rectangles in the stack is the subregion of R where the zeros have not been located. The second step would not stop until S_0 was found to be equal to one, then S_1 was computed, which would be the initial approximation for secant iteration. After this step the computation would return to the second step to continue finding the other zeros in the rest subregions. The calculation would stop if the stack of subregions was empty, otherwise it would repeat the second step. Besides, some other techniques like adaptive choice of step size and error control can be used to make the approach more reliable and highly efficient [29].

3.2. An example of application of winding number integral approach

As a demonstration of this approach, a wave propagation problem of circular duct with liner is taken as an example. Consider a circular duct with a non-locally reacting liner, the sound propagation would be decided by wave equation and boundary conditions. In a cylindrical coordinate system, a transcendental complex equation about radial wave number α could be obtained in the form of

$$F(\alpha) = 1 + \eta \left[\left(1 - Ma_x \frac{k_x}{k} \right)^2 \frac{\mathrm{J}_m(\alpha r_1)}{\alpha \mathrm{J}'_m(\beta r_1)} - \frac{1}{\beta} \frac{\mathrm{J}_m(\beta r_1)\mathrm{Y}'_m(\beta r_2) - \mathrm{J}'_m(\beta r_2)\mathrm{Y}'_m(\beta r_1)}{\mathrm{J}'_m(\beta r_1)\mathrm{Y}'_m(\beta r_2) - \mathrm{J}'_m(\beta r_2)\mathrm{Y}'_m(\beta r_1)} \right] = 0 \tag{63}$$

where η is the effective compliance, the explanation of r_1 and r_2 in Ref. [29]. The relationship between axial and radial wave number is

$$\frac{k_x}{k} = \frac{-Ma_x \pm \sqrt{1 - (1 - Ma_x^2)(\alpha / k)}}{1 - Ma_x^2} \tag{64}$$

Eq. (63) is the eigenvalue equation that needs to be solved very carefully. In this equation, the eigenvalue is the radial wave number.

Several numerical approaches can be employed to solve this equation, like Newton-Raphson iteration method or Runge-Kutta integral method. The comparison between winding number integral approach and Runge-Kutta method is shown in Fig. 3. In Fig. 3, the x-axis and y-axis correspond to the real and imaginary part of k, respectively. As shown in Fig. 3, the results of two methods agree with each other exactly except when the radial mode number n is 2, where the result of Runge-Kutta method has a remarkable deviation. It can be verified that the results of Runge-Kutta method is wrong, while the results of winding number integral method is right.

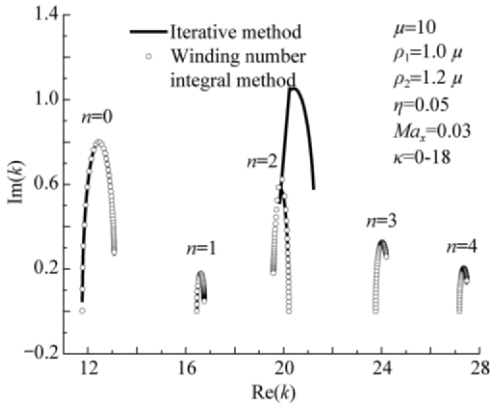

Fig. 3 Radial mode number of non-locally breacting liner in a cylinder duct.

This example shows that even for the solution of a very complicated dispersion equation like Eq. (63), winding number integral method could always precisely obtain the results in a designated region in the complex plane, which is also what we really need, especially for seeking the physical solution of the stability equation. That is why we try to extend this tool to be suitable for our stability model in matrix form.

4. Numerical Prediction and Experimental Results

4.1. Inception prediction of a low speed compressor

Our first validation of the model is to predict the stall

inception of a low speed axial compressor. The characteristic data and geometry of the compressor are required as input to the stall inception model, and all necessary data are available in the experiment which was conducted by Ludwig and Nenni [12]. This compressor has constant annular area with a hub-tip ratio of 0.80, and stagger angles 40° and 28.2°, chord length 3.7 cm and 3.3 cm for rotor and stator respectively. In the test, the mean axial flow velocity, U_0, was held constant at 18.3 m/s, while rotor speed was continuously variable between 500 r/min and approximately 1 700 r/min. Fig. 4 is the experimental curves from Refs. [10]-[12], which will be used in the present model.

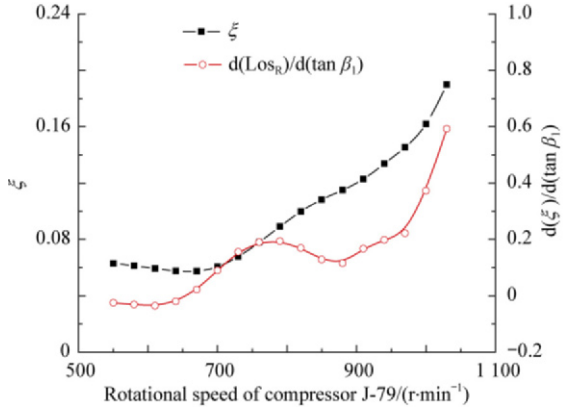

Fig. 4 Relative total pressure loss coefficient of rotor of J-79 and its derivatives to inlet flow angle.

Because the experiments were designed to investigate whether interference between a rotor and a stator has an impact on the inception of rotating stall, there were two sets of tests: one was rotor only, the other was a rotor-stator stage. In the test, the onset points of rotating stall were 1 000 r/min and 1 030 r/min for the rotor only and rotor-stator stage, respectively. The prediction given by our model is shown in Fig. 5. The x-axis represents the rotational speed of the rotor and y-axis represents the damping factor of the precursor wave, which has a definition $r_m\omega_I/mU_0$(ω_I is the imagiary of ω). There are two lines in Fig. 5, which correspond to the two sets of tests respectively, and theoretical stall inception occurs when the damping factor first goes to zero. The arrows in Fig. 5 point to the onset speed in the experiment. It was noted that the stall inception happened firstly on the first harmonic wave by the experimental observation, so does our theoretical prediction. Therefore, only the result for the first harmonic wave is shown in Fig. 5. It can be seen that both theoretical predictions of rotor-only and rotor-stator stage agree very well with experimentally observed inception points, and errors are no more than 10 r/min.

As for the propagation velocity of the perturbation wave for the two cases, the theoretical results are about 0.6 and 0.4 near the stall point, while the propagation

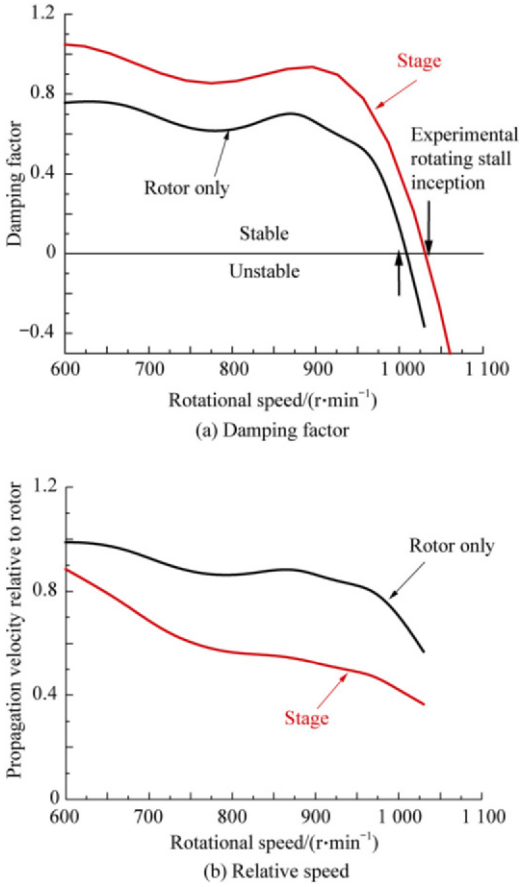

Fig. 5 Stability prediction of a low speed axial flow compressor J-79 (mode number (1,1)).

velocities of rotating cell are around 0.4 and 0.65 in the experiment.

It seems that theory and experiment do not agree with each other well. However, it could be seen that the discrepancy between Ludwig's theory [12] and the experiment was larger. His theoretical results were around 0.57 and 1.14, respectively. The reason may be that the propagation velocity of precursor wave or the frequency of the harmonic wave closely relates to the flow details except the matching conditions given in this model. So, any accurate prediction will require more flow details to be included in the stability model.

4.2. Stall inception's prediction of NASA Rotor 37 at 70% design rotational speed

In this section, the inception of rotating stall for a high speed compressor is predicted based on a typical example, i.e., NASA Stage 37 [40]. The purpose of this calculation is to test the ability of the model for high speed compressors without considering transonic case. So the data at 70% design rotational speed is used as the input parameters, and the inlet relative Mach number is between 0.8 and 1.0. The details of the

geometries and characteristics can be referred to NASA report [40].

The prediction results take the same form as the last section, i.e. propagation speed and damping factor of the perturbation frequency. As shown in Fig. 6, there are three lines, which represent the three different modes (*m*, *n*), i.e, (1, 1), (2, 1) and (3, 1), respectively. It is seen from Fig. 6(b) that the dimensionless perturbation velocity ranges from 0.50 to 0.75 for the three modes. The arrow labeled by "E" in Fig. 6(a) points to the experimental onset point of rotating stall. The arrow labeled by "T" points to the onset point predicted by the model. The difference of flow coefficient between theory and experiment is about 0.02, while the relative error is about 5.4%. It was not known from the experiment which mode corresponded to the inception point of rotating stall. From our theoretical prediction it seems to be the first circumferential mode that goes to neutral point in advance in Fig. 6(a), and the other two modes are slightly more stable than the first mode. This investigation shows that the present model is capable of being used to predict the stall inception for high subsonic fan/compressors.

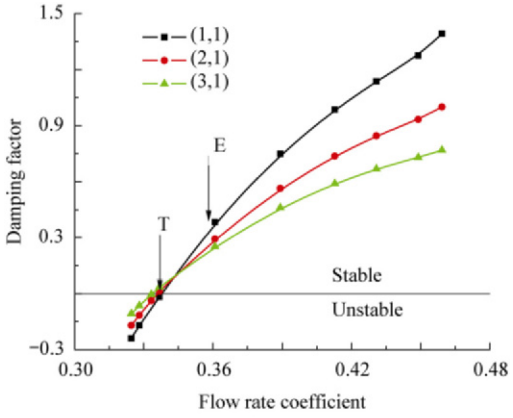

(a) Damping factor

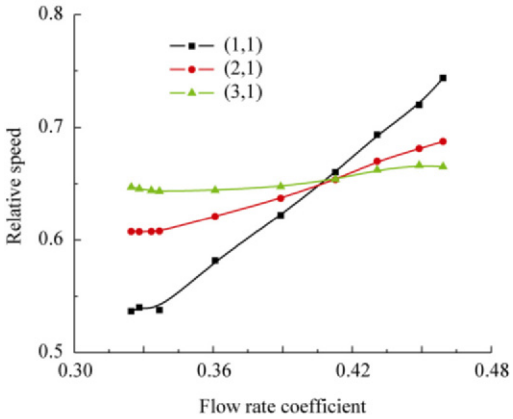

(b) Relative speed

Fig. 6 Stability prediction of NASA Rotor 37 at 70% design rotational speed (mode number (1,1), (2,1), (3,1)).

4.3. *Stall inception's prediction of NASA Rotor 37 at 100% design rotational speed*

The third example is to validate the modified semi-actuator model for transonic fan/compressors. The chosen object is still NASA Stage 37, but the speed moves up to 100% design rotational speed. In this situation, the inlet Mach number has been increased to a range from 1.2 to 1.4, and then the stage becomes a typical transonic compressor. To predict the inception of rotating stall, the first thing is to extract experimental data for the work [40]. As mentioned previously, some simplifications and assumptions have to be taken. For a real three-dimensional compressor, the actual flow incidence varies with the radius and the inlet relative Mach numbers are also different along the span of blade. So, in order to make use of the present model, the experimental data has to be averaged in the radial direction to obtain the relative mean Mach number at the inlet. Besides, the Mach number right before the in-passage shock is determined by using the Prandtl-Meyer function. The Mach number after the shock wave is obtained by using the Rankin-Hugniot relations, and then the total pressure loss can be known. So it has to be pointed out that this procedure and the obtained data may just qualitatively reflect some key flow features, which inevitably neglect many physical details related to complicated transonic flow in cascade passage. Fig. 7 is the input data that the present model requires, which is obtained from the experimental results [40]. Fig. 8 is the predicting result for different mode combinations. This result shows that the different combinations of the three circumferential mode numbers with the first radial mode number is the most sensitive modes related to the inception point. In fact, the predicted stall inception quite approaches the experimental data as shown in Fig. 8. The present model includes both the effect of both shock loss and reflection on various pressure waves. From the predicting results, it seems that the main physical features of the stall inception for transonic fan/compressors can be captured in this way.

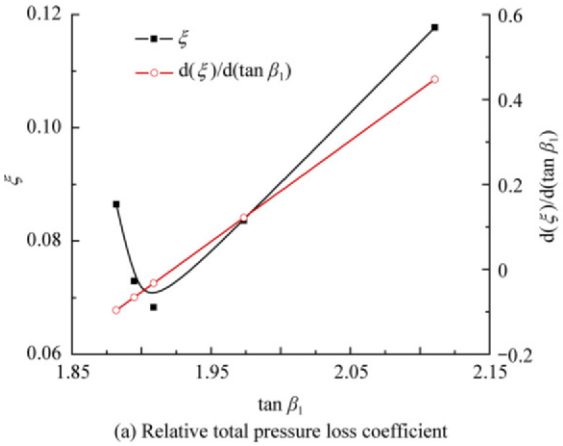

(a) Relative total pressure loss coefficient

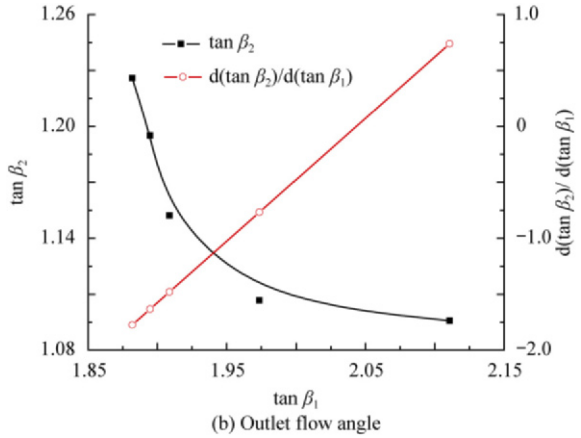

(b) Outlet flow angle

Fig. 7 Characteristics of rotor of NASA Stage 37 and its derivatives to the inlet flow angle at 100% design rotational speed.

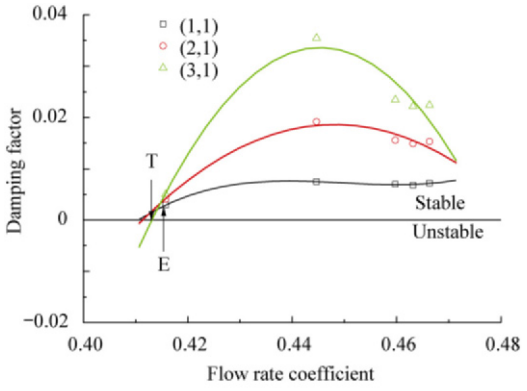

(a) Damping factor

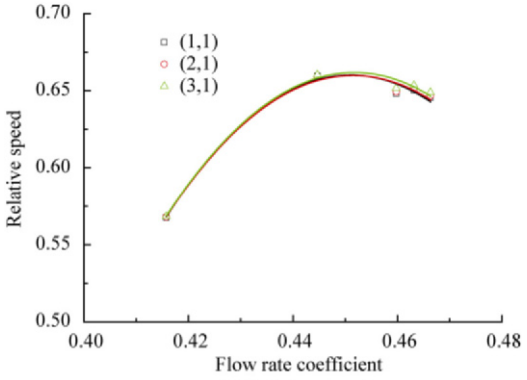

(b) Relative speed

Fig. 8 Stability prediction of NASA Stage 37 at 100% design rotational speed (mode number (1,1), (2,1), (3,1)).

4.4. Experimental investigations and various comparisons for TA36 Fan

Some experimental researches have been conducted based on a low speed fan designed by ourselves. The experimental facility is show in Fig. 9 and the main design parameter for TA36 Fan is displayed in Table 1 and Table 2.

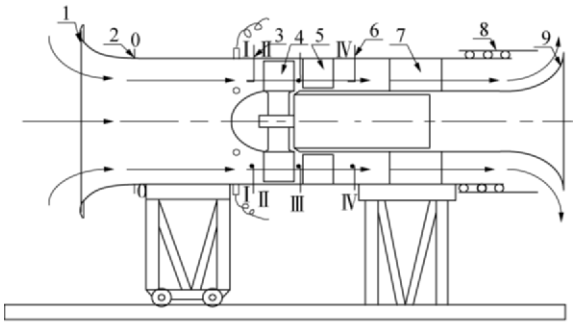

1—Flow tube; 2—Measurement point of wall static pressure; 3—Measurement point of inlet total pressure; 4—Rotor; 5—Stator; 6—Measurement point of outlet total pressure and static pressure; 7—Motor; 8—Struts; 9—Outlet adjusting mechanism.

Fig. 9 Schematic of TA36 Fan.

Table 1 Geometrical parameters for TA36 Fan

Parameter	Rotor	Stator
No. of blades	20	27
Tip diameter/mm	600	600
Hub to tip ratio	0.577	0.669
Tip stagger angle/(°)	45	0

Table 2 Aerodynamic parameters for TA36 Fan

Parameter	Value	Parameter	Value
Mass flow/(kg·s^{-1})	6.5	Design speed/(r·min^{-1})	2 900
Efficiency/%	85	Total pressure ratio	1.022
Stall margin/%	15.5	Total pressure rise/Pa	2 000

We have two different ways to obtain the performance parameters for this fan, the first is to use CFD method to calculate the characteristic line and total pressure loss, etc., the second is to measure all the parameters based on the relevant experiment. From Fig. 10, it is seen that the results from CFD and experimental data have clear differences for each performance curves. But the basic tendency is almost the same. On the basis of these data, the prediction of inception point of the fan is nearly same as shown in Fig. 11(a). However it can also be noted that the relative propagation speed of the precursor has remarkable difference as shown in Fig. 11(b). It is seen again that it is quite important to include more flow details in the model if one expects the propagation speed to be predicted more accurately. Besides, it is well known that the calculation of performance of fan/compressors is based on steady CFD method or other empirical models, and it is extremely difficult to

accurately determine the stall margin during design stage. Perhaps, we can finish some preliminary stability design in this way if the stall inception point can be predicted well with the help of the stall inception model and the steady flow simulation. Our example only shows such possibility for further application. In Fig. 10, p_1^* is the inlet stastic pressure, p_2 the outlet total pressure, M the mass flow.

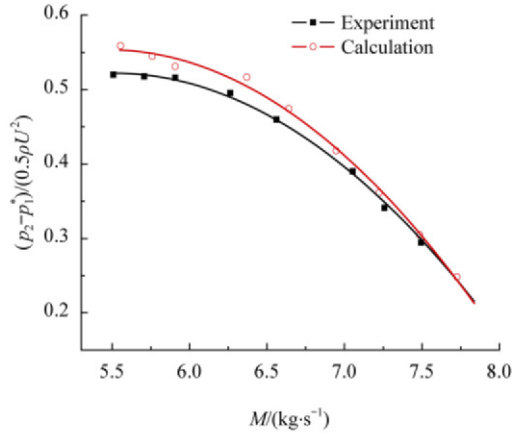

(a) Pressure rise coefficient

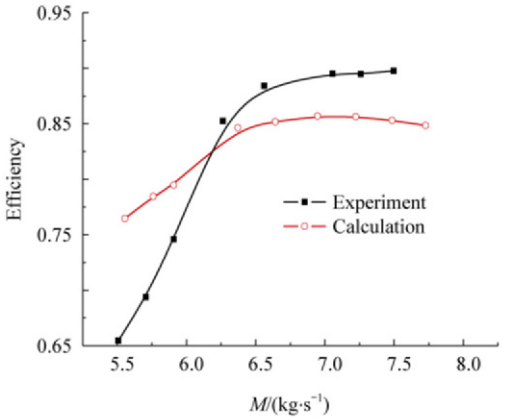

(b) Efficiency

Fig. 10 Characteristics of TA36 Fan.

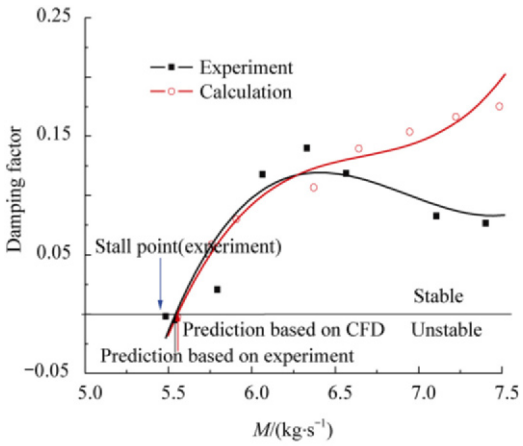

(a) Damping factor

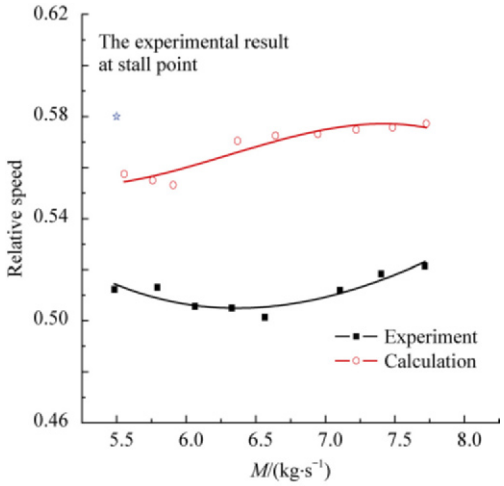

(b) Relative speed

Fig. 11 Stability prediction of TA36 Fan at 100% design speed.

5. Conclusions

(1) A transonic compressible stability model for axial flow fan/compressors is presented. Based on the analysis of the unsteady phenomenon caused by casing treatments, the function of casing treatments has been modeled by a wall impedance condition which has been involved in the stability model through the eigenvalues and the corresponding eigenfunctions of the system. Besides, the effect of shock waves in cascade channel on the stability prediction is also considered in the present model.

(2) Various numerical results show that the present stability model can give a reasonable prediction to the stall inception point for both subsonic and transonic fan/compressors. Especially, the present experimental data also shows a good agreement with the predicting result by use of the input parameters either from the experimental measurement or from steady CFD calculation. This means that we may carry out the stability design on the basis of steady CFD calculation with the help of the stall inception model in order to guarantee enough stall margin of fan/compressors during design phase.

(3) As for the effect of casing treatment on the stall inception, we will give more theoretical and experimental results in a separated paper. Besides, the present model has not considered the effect of annular domain, neglecting the centrifugal affect and radial mean velocity. It is also required to include more flow and geometrical parameters in the stall inception model for any more accurate prediction.

References

[1] Epstein A H, Ffowcs-Williams J E, Greitzer E M. Active suppression of compressor instabilities. AIAA-1986-1914, 1986.

[2] Paduano J D, Greitzer E M, Epstein A H. Compression system stability and active control. Annual Review of

Fluid Mechanics 2001; 33: 491-517.
[3] Day I J. Active suppression of rotating stall and surge in axial compressors. ASME Paper 1991-GT-87, 1991.
[4] Day I J. Review of stall, surge and active control in axial compression system. ISABE 1993-7011, 1993.
[5] Escuret J F, Garnier V. Numerical simulations of surge and rotating stall in multi-stage axial flow compressors. AIAA-1994-3202, 1994.
[6] Gong Y, Tan C S, Gordon K A, et al. A computational model for short wavelength stall inception and development in multi-stage compressors. ASME Journal of Turbomachinery 1999; 121(4): 726-734.
[7] Longley J P. Calculating the flow field behaviour of high-speed multi-stage compressors. ASME Paper 1997-GT-468, 1997.
[8] He L. Computational study of rotating-stall inception in axial compressors. Journal of Propulsion and Power 1997; 13(1): 31-38.
[9] Han C, Bergner J, Schiffer H. Short length-scale rotating stall inception in a transonic axial compressor, criteria and mechanism. ASME Paper 2006-GT-90045, 2006.
[10] Nenni J P, Ludwig G R. A theory to predict the inception of rotating stall in axial flow compressors. AIAA-1974-528, 1974.
[11] Sears W R. Rotating stall in axial compressors. Zeitschrift Fur Angewandte Mathematik Und Physik 1955; 6(6): 429-454.
[12] Ludwig G R, Nenni J P. Basic studies of rotating stall in axial flow compressors. AFAPL-TR-1979-2083, 1979.
[13] Greitzer E M. Surge and rotating stall in axial flow compressors: part Ⅰ, Ⅱ. ASME Journal of Engineering for Power 1976; 98(2): 190-217.
[14] Moore F K. A theory of rotating stall of multistage axial compressors: part Ⅲ, Ⅳ. ASME Journal of Engineering for Gas Turbine and Power 1984; 106(2): 313-334.
[15] Moore F K, Greitzer E M. A theory of post-stall transients in axial compression systems: part Ⅰ, Ⅱ. ASME Journal of Engineering for Gas Turbine and Power, 1986; 108(2): 68-75, 231-239.
[16] McCaugham F E. When are nonlinearities important at stall inception? ASME Paper 1994-GT-338, 1994.
[17] Hendricks G J, Bonnaure L P, Longley J P, et al. Analysis of rotating stall onset in high speed axial flow compressors. AIAA-1993-2233, 1993.
[18] Feulner M R, Hendricks G J, Paduano J D. Modeling for control of rotating stall in high speed multi-stage axial compressors. ASME Paper 1994-GT-2, 1994.
[19] Takata H, Nagashima T. Rotating stall in three-dimensional blade rows subjected to spanwise shear flow. ISABE 1985-7008, 1985.
[20] Gordon K. Three-dimensional rotating stall inception and effects of rotating tip clearance asymmetry in axial compressors. PhD thesis, Massachusetts Institute of Technology, 1998.
[21] Namba M. Three-dimensional flows. Platzer M F, Carta F O. AGARD Manual on Aeroelasticity in Axial Flow Turbomachinery: Vol.1, Unsteady Turbomachinery Aerodynamics. AGARD- AG-298, 1987.
[22] Watanabe T, Kaji S. Possibility of cascade flutter suppression by sse of non-rigid duct walls. The Symposium Proceedings of Unsteady Aerodynamics of Turbomachines and Propellers. 1984; 261-276.
[23] Kaji S, Okazaki T. Propagation of sound waves through a blade row: I. analysis based on the semi-actuator disk theory. Journal of Sound and Vibration, 1970; 11(3): 339-353.
[24] Zorumski W E. Acoustic theory of axisymmetric multisectioned ducts. NASA TR R-419, 1974.
[25] Kraft R E. Adjointness properties for differential systems with eigenvalue dependent boundary conditions with apllication to flow duct acoustics. Journal of Acoustical Society of America 1977; 61(4):913-922.
[26] Joshi M C, Kraft R E, Son S Y. Anaylsis of sound propagation in annular ducts with segmented ducts with segmented treatment and sheared flow. AIAA-1982-0123, 1982.
[27] Micklow J, Jeffers J. Semi-actuator disk theory for compressor choke flutter. NASA-CR-3426, 1981.
[28] Brazier-Smith P R, Scott J F. On the determination of the dispersion equations by use of winding number integrals. Journal of Sound and Vibration 1991; 141: 503-510.
[29] Ivansson S, Karasalo I. Computation of modal numbers using an adaptive winding-number integral method with error control. Journal of Sound and Vibration 1993; 161: 173-180.
[30] Ko S H. Sound attenuation in acoustically circular ducts in the presence of uniform flow and shear flow. Journal of Sound and Vibration 1972; 22: 193-210.
[31] Sun X F. On the relation between the inception of rotating stall and casing treatment. AIAA-1996-2579, 1996.
[32] Bechert D W. Sound absorption caused by vorticity shedding, demonstrated with a jet flow. Journal of Sound and Vibration 1980; 70: 389-405.
[33] Howe M S. Attenuation of sound in a low Mach number nozzle flow. Journal of Fluid Mechanics 1979; 91: 209-229.
[34] Howe M S. On the theory of unsteady high Reynolds number flow through a circular aperture. Proceedings of the Royal Society London A366. 1979; 205-223.
[35] Dowling A P, Hughes I J. Sound absorption by a screen with regular array of slits. Journal of Sound and Vibration 1992; 156: 387-405.
[36] Hughes I J, Dowling A P. The absorption of sound by perforated linings. Journal of Fluid Mechanics 1990; 218: 299-335.
[37] Jing X D, Sun X F. Experimental investigations of perforated liners with bias flow. Journal of the Acoustical Society of America 1999; 106(5): 2436-2441.
[38] Jing X D, Sun X F. Effect of plate thickness on impedance of perforated plates with bias flow. AIAA Journal 2000; 38(9): 1573-1578.
[39] Sun X F, Jing X D, Zhao H W. Control of blade flutter by smart-casing treatment. Journal of Propulsion and Power 2001; 17(2): 248-255.
[40] Moore R D, Reid L. Performance of single-stage axial flow transonic compressor with rotor and stator aspect ratios of 1.19 and 1.26, respectively, and with design pressure ratio of 2.05. NASA TP-2001, 1980.

Biographies:

SUN Xiaofeng Born in 1962, he is a professor in Beihang University. His main research interests are flow stability of fan/compressor and combustion, acoustic design of modern passenger aircraft.
E-mail: sunxf@buaa.edu.cn

SUN Dakun Born in 1981, he received Ph.D. degree from Beihang University in 2010. His main research interest is flow stability of compressor.
E-mail: renshengming@sjp.buaa.edu.c